View metadata, citation and similar papers at core.ac.uk

brought to you by CORE

provided by PORTO Publications Open Repository TOrino

Post print (i.e. final draft post-refereeing) version of an article published on *Engineering Fracture Mechanics*. Beyond the journal formatting, please note that there could be minor changes from this document to the final published version. The final published version is accessible from here:
http://dx.doi.org/10.1016/S0013-7944(02)00041-3
This document has made accessible through PORTO, the Open Access Repository of Politecnico di Torino (http://porto.polito.it), in compliance with the Publisher's copyright policy as reported in the SHERPA-ROMEO website:
http://www.sherpa.ac.uk/romeo/issn/0013-7944/

Creep and Fracture in Concrete: A Fractional Order Rate Approach

F. Barpi* and S. Valente†

*Assistant Researcher, Department of Structural and Geotechnical Engineering, Politecnico di Torino, Corso Duca degli Abruzzi 24, 10129 Torino, Italy.
Tel: +39 11 5644886, Fax: +39 11 5644899, e-mail: *barpi@polito.it*,

†Professor, Department of Structural and Geotechnical Engineering, Politecnico di Torino, Corso Duca degli Abruzzi 24, 10129 Torino, Italy.
Tel: +39 11 5644853, Fax: +39 11 5644899, e-mail: *valente@polito.it*

Keywords Cohesive, Concrete, Crack, Creep, Fracture, Fractional, Long-term behaviour, Softening, Viscosity.

Abstract *The paper analyses the interaction between strain-softening and time-dependent behaviour in the case of quasi-static fracture of concrete. A viscous element based on a fractional order rate law is coupled with a micromecanical model for the fracture process zone. This approach makes it possible to include a whole range of dissipative mechanisms in a single rheological element. Creep fracture in mode I conditions is analysed through the finite element method, the cohesive (or fictitious) crack model and a new space and time integration scheme. The comparison with creep tests executed on three-point bending conditions shows a good agreement.*

1 INTRODUCTION

The long term performance of concrete structures is fundamentally affected by the behaviour of the material after cracking. It is well known that concrete presents a diffused damage zone within which micro-cracking increases and stresses decrease as the overall deformation increases. This results in the softening of the material in the so called *fracture process zone* (FPZ). The size of this zone can be compared with a characteristic dimension of the structure and can vary during the evolutionary process. In this context, a numerical method (based on finite or boundary elements) has to be used together with the *cohesive* or *fictitious* crack model as shown by Barenblatt [1], Dugdale [2] and Hillerborg [3].

The interaction between strain-softening and time dependent behaviour is analysed, with the emphasis on very slow or quasi-static fracture. This is the case of cracking in massive concrete structures like dams, where inertial forces can be neglected. This approach is based on a *micromechanical* model which combines time-dependent and time-independent information. One of these models was proposed by Santhikumar and Karihaloo [4, 5]. The time-independent part of this model is based on the concept of *effective spring*, which derives from a micromechanical hypothesis for the static softening behaviour of the concrete in the fictitious process zone proposed in [6]. In the present paper this approach is enhanced using a *fractional order rate* law and is applied to the numerical simulation of the three-point bending tests described by Zhou [7].

The proposed approach can be compared with the one proposed in [8] (rate dependent softening) and the one proposed in [9] (stress relaxation law in the FPZ obtained by fitting stress relaxation test results).

2 RHEOLOGICAL MODEL

Rheology is concerned with time dependent deformation of solids. In the simplest rheological model of the linear standard viscoelastic solid (Fig. 1), the springs are characterized by linear stress-displacement relationships:

$$\sigma_1 = E_1\,(\varepsilon - \varepsilon_1), \tag{1a}$$

$$\sigma_2 = E_2\,\varepsilon. \tag{1b}$$

The dashpot is based on the following *fractional order rate* law for the internal variable ε_1:

$$D^\alpha \varepsilon_1 = \frac{\mathrm{d}^\alpha \varepsilon_1}{\mathrm{d}t^\alpha} = \frac{\sigma_1}{E_1\,\tau_1^\alpha} = \frac{\varepsilon - \varepsilon_1}{\tau_1^\alpha} \quad \text{with} \quad \alpha \in (0,1), \tag{2}$$

where the fractional differentiation of a function $y(t)$ is defined according to [10, 11] (see the Appendix for more details).

Equation 2 represents a generalization of the well-known Newton's constitutive law for the dashpot:

$$\sigma = \eta \frac{\mathrm{d}\varepsilon}{\mathrm{d}t} = E\,\tau\,\frac{\mathrm{d}\varepsilon}{\mathrm{d}t}, \quad \text{or, to compare with Eq. 2:} \quad \frac{\mathrm{d}\varepsilon}{\mathrm{d}t} = D^1\varepsilon = \frac{\sigma}{E\,\tau}. \tag{3}$$

In Eq. 2 the classical derivative of integer order ($\alpha = 1$) of the deformation ε is replaced by a derivative of order α and, to maintain the correct dimensions, the relaxation time τ_1 is changed by τ_1^α.

In particular, the non integer (of order m) differential operator $D^m\, y(t)$ is defined as:

$$D^{-(1-\alpha)}\, y(t) = \int_0^t \Phi_{1-\alpha}(t-\bar{t})\; y(\bar{t})\mathrm{d}\bar{t}, \tag{4}$$

where:

$$\Phi_{1-\alpha}(t) = \frac{t_+^{-\alpha}}{\Gamma(1-\alpha)} \quad \text{with} \quad t_+ = \begin{cases} t & \text{if} \quad t > 0 \\ 0 & \text{if} \quad t < 0 \end{cases}. \tag{5}$$

In the previous expression Γ represents the *Gamma function*. Equation 4 can also be obtained by using an hereditary model based on a *Rabotnov fractional exponential kernel* [12].

A convergent expression for the α-order fractional derivative operator D^α is given by:

$$D^\alpha y(t) = D^1 D^{-(1-\alpha)} y(t) =$$

$$\frac{\mathrm{d}}{\mathrm{d}t}\int_0^t \Phi_{1-\alpha}(t-\bar{t})\; y(\bar{t})\mathrm{d}\bar{t} = \frac{1}{\Gamma(1-\alpha)}\,\frac{\mathrm{d}}{\mathrm{d}t}\int_0^t \frac{y(\bar{t})}{(t-\bar{t})^{-\alpha}}\mathrm{d}\bar{t}. \tag{6}$$

In the case of $\alpha = 1$ the classical dashpot with an integer order rate law is obtained from Eq. 2. In particular, the solutions for the relaxation problem (under constant w) and for the creep problem (under constant σ) become of exponential type, with τ_1 as the *relaxation time*, and $\tau_1 \frac{E_1+E_2}{E_2}$ as the *retardation time*. A comparison between the solutions corresponding to α integer and α non integer is plotted in Fig. 2 and 3.

2.1 Numerical integration of constitutive response

A possible approximation for the fractional differentiation of a function $y(t)$ is [10]:

$$^{n+1}(D^\alpha y) = \frac{1}{(\Delta t)^\alpha}\sum_{j=0}^{n} b_j(\alpha)\; {}^{n+1-j}y. \tag{7}$$

It is assumed that the spacing in time is uniform, i.e., $^n y = y(n\Delta t)$. The coefficients $b_j(\alpha)$ depend on the Gamma function as follows:

$$b_j(\alpha) = \frac{\Gamma(j-\alpha)}{\Gamma(-\alpha)\,\Gamma(j+1)}. \tag{8}$$

By using the recursion formula:

$$\frac{\Gamma(j-\alpha)}{\Gamma(j+1)} = \frac{(j-1-\alpha)}{j}\frac{\Gamma(j-1-\alpha)}{\Gamma(j)}, \tag{9}$$

no evaluation of Gamma function is needed and the coefficients $b_j(\alpha)$ are given by:

$$b_0(\alpha) = 1, \quad \ldots \quad b_k(\alpha) = \frac{(k-1-\alpha)}{k}\; b_{k-1}(\alpha), \quad \ldots \quad k = 1, \ldots, n. \tag{10}$$

For convenience, the expression in Eq. 7 can be rewritten as:

$$^{n+1}(D^\alpha y) = \frac{1}{(\Delta t)^\alpha}(^{n+1}y - {}^{n}\overline{y}), \tag{11}$$

where

$$ {}^{n}\overline{y} = -\sum_{j=1}^{n} b_j(\alpha)\, {}^{n+1-j}y, \tag{12} $$

is a known quantity at time t_{n+1}.

At this point the updated stress quantities ${}^{n+1}\sigma$ can be obtained by using Eq. 11 with reference to Eq. 2. The integration over time is executed with the classical *General Midpoint Rule* [13].

3 MICROMECHANICAL MODEL FOR THE PROCESS ZONE

In each point of the fictitious process zone a micromechanical approach to tension softening is combined with the above rheological model (described in Fig. 1 and Eq. 2) according to a method proposed in [4, 5]. Tension softening behaviour appears when the damage in the material has localized along eventual fracture planes: this behaviour has been successfully modelled using two- and three-dimensional micromechanical models [6, 12].

3.1 Loading phase

All models provide a relationship between the residual tensile stress carrying capacity σ[1] and crack opening displacement w (also called COD) as a function of known concrete microstructural parameters (included in the factor β), e.g. aggregate volume fraction V_f, Young's modulus E_c, ultimate tensile strength f_t and fracture toughness of the homogenized material K_{Ic}^{hom} (see Fig. 4).

According to these models, the function is assumed to be:

$$ \frac{w}{w_c} = \frac{(K_{Ic}^{hom})^2}{E_c(1-V_f)f_t}\,\frac{f_t}{\sigma}\left[1-\left(\frac{\sigma}{f_t}\right)^3\right] = \beta\,\frac{f_t}{\sigma}\left[1-\left(\frac{\sigma}{f_t}\right)^3\right]. \tag{13} $$

3.2 Creep phase

During the creep phase (at constant load), the $(\sigma - w)$ law is generalized in the same way of Eq. 3; the deformations ε and ε_1 are now replaced by the crack opening displacements w and w_1. By using a fractional order rate law it is possible to write:

$$ D^{\alpha} w_1 = \frac{\mathrm{d}^{\alpha} w_1}{\mathrm{d}t^{\alpha}} = \frac{\sigma_1}{K_1\,\tau_1^{\alpha}} = \frac{w - w_1}{\tau_1^{\alpha}} \quad \text{with} \quad \alpha \in (0,1), \tag{14} $$

where the constants K_1 and K_2 are defined in the following Sections and in Fig. 5. They represent the counterpart of the elastic moduli E_1 and E_2 of the classical viscoplastic model[2]. In the present work $K_1 = K_2$ is assumed.

[1] From here to the end of the paper, σ indicates the *stress* in the *cohesive zone*.

[2] Notice that the physical dimensions of K_1 and K_2 differ from those of an elastic modulus.

4 RHEOLOGICAL AND MICROMECHANICAL MODEL INTERACTION

During the loading phase each point of the FPZ moves on the same $(\sigma - w)$ curve. Later on this condition does not hold any longer, due to the combined effect of *viscosity* and *damage*.

In order to understand how the rheological and micromechanical models interact, three *single degree of freedom* systems were presented in [4, 5], in the case of integer rate law.

1. In the case of the first system, the displacement discontinuity w is kept constant along time step Δt; the stress relaxation $\Delta\sigma$ occurs according to the standard viscoelastic model described. Each stress relaxation $\Delta\sigma$, through the unloading stiffness hypothesis (Fig. 5, centre), induces an istantaneous stiffness reduction (*effective spring* concept) related to the time increment Δt.

2. In the case of the second system, the stress σ is kept constant along time step Δt; the creep displacement Δw occurs according to the standard viscoelastic model described. Each creep displacement increment Δw, through the tangential softening hypothesis (Fig. 5, right), induces an istantaneous softening reduction related to the time increment Δt.

3. In the case of the third system, both stress σ and displacement discontinuity w are forced to stay on the static curve (Eq. 13). One of the two increments ($\Delta\sigma$ or Δw) occurs as predicted by the rheological model, while the other is smaller or equal to the value predicted by the rheological model.

At the end of each time step, the microcrack pattern changes and, in either case, stiffness is reduced.

In the present work, a *multiple degree of freedom* system is analized. Therefore, the above mentioned approach were generalized through the Finite Element method as described in the following Sections. It is worth noting that each point in the FPZ follows a different path and, hence, exhibits a different stiffness, while $K_1 = K_2$.

5 FINITE ELEMENT ANALYSIS

In the present work, the continuum surrounding the process zone is assumed as *linear elastic*. All non-linear and time-dependent phenomena are assumed to occur in the *process zone*. When the fictitious crack tip (F.C.T.) advances by a pre-defined length, each point located on the crack trajectory, is split into two points. The virtual mechanical entity, acting on these two points only, is called *cohesive element*. The local behaviour of such an element follows the rules mentioned in the previous section. Each cohesive element interacts with the others only through the undamaged continuum, external to the process zone.

According to the finite element method, by taking the unknowns to be the n nodal displacement increments, $\Delta\boldsymbol{u}$, and assuming that compatibility and equilibrium conditions are satisfied at all points in the solid, it is possible to obtain the following system of n equations with $(n+1)$ unknowns ($\Delta\boldsymbol{u}$, $\Delta\lambda$ or Δt). The creep effect is incorporated by simply adding the pseudo-load induced by relaxation to the load vector in the equilibrium equations [14, 15]:

$$(\boldsymbol{K}_T + \boldsymbol{C}_T)\,\Delta\boldsymbol{u} = \Delta\lambda\,\boldsymbol{P} + \Delta t\,\boldsymbol{Q}, \tag{15}$$

where:

- $\boldsymbol{K}_T$: positive definite tangential stiffness matrix, containing contributions from linear elastic (undamaged) elements and possible contributions from cohesive elements having (σ, w) below the curve of Fig 4. The conditions in which this possibility applies will be described later on;
- $\boldsymbol{C}_T$: negative definite tangential stiffness matrix, containing contributions from cohesive elements with (σ, w) on the curve of Fig 4;
- $\boldsymbol{P}$: the vector of external load;
- $\Delta\lambda$: maximum load multiplier which is compatible with Eq. 13 and the fictitious crack tip growth condition ($\sigma_{F.C.T.} = f_t$);
- $\boldsymbol{Q}$: vector of unbalanced load (or pseudo-load) due to relaxation in the process zone, related to a unitary time increment.

During the loading phase, the behaviour of the material is assumed to be time-independent ($\boldsymbol{Q} = \boldsymbol{0}$), the external load changes, $\Delta\lambda \neq 0$, and $\Delta t = 0$. On the contrary, during the sustained loading phase, the behaviour of the process zone is assumed to be time-dependent ($\boldsymbol{Q} \neq \boldsymbol{0}$), the external load is kept constant, $\Delta\lambda = 0$, and $\Delta t \neq 0$.

5.1 Interaction between cohesive elements

During the loading phase, all the stress paths in the FPZ are forced to follow the $(\sigma - w)$ law (defined Eq. 13). For the boundary condition analysed dw is *always* and *everywhere* positive. A more complex situation occurs during the next loading phase (*sustained*): the unloading stiffness approaches ∞ when w tends to 0^+. In order to avoid this difficulty, a threshold value has to be assumed for w. A cohesive element is classified as *active*, and submitted to the rheological model, when and only when its w is bigger than the threshold, assumed equal to $0.001 w_c$. Otherwise the stress path is forced to follow the $(\sigma - w)$ law as it occurs during the loading phase.

According to the rheological model, for each active cohesive element, it is possible to compute the stress relaxation under constant w ($\mathrm{d}\sigma_t$) as well as the creep displacement under constant σ ($\mathrm{d}w_t$). It is important to notice that $\mathrm{d}\sigma_t$ and $\mathrm{d}w_t$ are *threshold values* computed according to the micromechanical model, while $\mathrm{d}\sigma$ and $\mathrm{d}w$ are *real values* obtained from equilibrium and compatibility conditions.

The compatibility conditions can be grouped in the following cases :

1. full relaxation only: $\mathrm{d}\sigma = \mathrm{d}\sigma_t < 0$ and $\mathrm{d}w < \mathrm{d}w_t$ (see segment AB in Fig. 5);
2. full creep only: $\mathrm{d}\sigma < \mathrm{d}\sigma_t < 0$ and $\mathrm{d}w = \mathrm{d}w_t$ (see segment BC in Fig. 5);
3. full creep with elastic increment: $\mathrm{d}\sigma = (\mathrm{d}w - \mathrm{d}w_t)\, K_1 > 0$ and $K_1 > 0$ and $\mathrm{d}w > \mathrm{d}w_t$ (see segment CD in Fig. 5);
4. full creep with softening increment: $\mathrm{d}\sigma = (\mathrm{d}w - \mathrm{d}w_t)\, K_1 < 0$ and $K_1 < 0$ and $\mathrm{d}w > \mathrm{d}w_t$ (see segment CF in Fig. 5).

In order to follow this process of classification, an inner loop must be introduced. Since the incremental problem is formulated as linear with threshold, each *physical* time step has to be divided into numerous *logical* substeps. When case (3) or (4) are applied, stiffness

matrix coefficients are changed from one substep to the next [14, 15]. Otherwise they are kept constant during all the substep iterations.

Creep rupture time is reached when the smallest eigenvalue of the tangential stiffness matrix becomes negative: this means that the external load can no longer be kept constant.

6 EXPERIMENTAL AND NUMERICAL RESULTS

The experimental tests, executed on prenotched beams, described in [7], were simulated numerically. The experimental procedure is based on two phases. In the first, the external load grows from zero to the nominal level (a fraction of the maximum load P_{max} taken equal to 0.76, 0.80, 0.85 and 0.92, see Fig. 7 and Fig. 8) under deflection control (5×10^{-6} m/s), while, during the second, the load is kept constant until the creep rupture occurs (*pre-peak* sustained bending).

These tests are usually associated with the name of *pre-peak sustained bending* tests. Of course, in order to know the maximum load $P_{max} \approx 900$ N, a number of static tests have to be previously executed. To overcome this difficulty, different authors prefer to use the so-called *post-peak* tests where the creep phase starts beyond the peak point [16, 17]. The specimen dimensions are $10 \times 10 \times 80$ cm, the notch depth is 5 cm, while the material properties, as described in [7], are presented in Table 1.

The numerical simulations were executed using the values listed in Table 2, and neglecting the time dependent behaviour of the undamaged material. The finite element mesh around the symmetry axis is presented in Fig. 6 while the dimension of the smallest elements is equal to $\frac{H}{160} = \frac{10}{160} = 0.625$cm. As suggested in [15] the following limit is applied to each step: $|\frac{\mathrm{d}\sigma}{f_t}| \leq 0.01$.

Figure 7 shows the experimental and numerical load vs. crack mouth opening displacement curves for static tests as well as for sustained load tests. Figure 8 shows the load level vs. the logarithm of the *failure lifetime* (creep rupture time), for different values of the fractional derivative order α (0.30 and 1.00). The best fitting of the experimental results is achieved assuming $\alpha = 0.30$. Experimental and numerical results appear to be in good agreement.

Finally, Figs. 9 and 10 show the stress distribution inside the process zone (the maximum value of tensile stress is f_t, according to the cohesive model) and the stress path followed from some cohesive elements during the external load growth ($\frac{P_{cost}}{P_{max}} = 0.92$). As explained before, the couples $(\sigma - w)$ are not restricted to stay on the static envelope.

7 CONCLUSIONS

- A *linear* viscoelastic rheological element, combined with a suitable *micromechanical* model is successfully used for studying Mode I crack propagation problems.

- A *single* rheological element has been used. *Four* material properties only, namely, the elastic constants K_1 and K_2, the relaxation time τ_1 and the order α of the fractional derivative are enough to describe the phenomenon. It is not necessary to use long chains of rheological elements, whose properties are difficult to determine.

- A *fractional order rate* makes it possible to include a *whole spectrum* of dissipative mechanisms in a *single* viscous element.

- A new time integration scheme is proposed. The incremental problem is formulated as *linear with threshold* with an upper limit to the initial values of the unloading

stiffness (when $\sigma \approx f_t$).

8 Appendix – Non integer derivative of the unit function

This Section presents, without proof, the results of the non integer differentiation (or, following Oldham and Spanier [10], "differintegral") of the *unit function* $y(x) = 1$. It is worth noting that, from a general viewpoint, the non integer derivative of $y(x) = 1$ is *not* equal to zero: the expected zero is obtained just for a *positive integer* α (α=1 and 2 in Fig. 11). For $\alpha = -1$ the integral function $Y(x) = x$ (i.e., $Y(x) = \frac{\mathrm{d}^{-1}y(x)}{\mathrm{d}x} = \int_0^x y(x)\,\mathrm{d}x = \int_0^x 1\,\mathrm{d}x = x$) is obtained (Fig. 11). For *non integer* values of α the remaining curves of Fig. 11 are obtained.

9 ACKNOWLEDGMENTS

The financial support provided by the Italian Department of Education, University and Scientific Research (MIUR) to the research project on *"Ultimate Limit State Structural Analysis of Concrete Dams"* (grant number MM08161945_005) is gratefully acknowledged.

10 Notation

- $\varepsilon, \varepsilon_1$: deformations of the rheological model
- σ: stress of the rheological model, stress in the cohesive zone
- σ_1: stress of the rheological model
- E_1, E_2: Young's moduli of the rheological model
- η: classical Newton's viscosity parameter
- $\tau_1 = \frac{\eta}{E_1}$: relaxation time
- $D^\alpha(\bullet) = \frac{\mathrm{d}^\alpha(\bullet)}{\mathrm{d}t^\alpha}$: fractional derivative operator of order α
- α: order of differentiation
- Γ: Euler's Gamma function $\left(\Gamma(x) = \int_0^\infty e^i\, t^{(x-1)}\mathrm{d}t = \lim_{n\to\infty} \frac{n^x\, n!}{x\,(x+1)...(x+n)}\right)$
- $y(t)$: generic function of time
- $\Phi_{1-\alpha}(t)$: kernel of the non integer differentiation definition
- $b_i(\alpha)$: i^{th} coefficient of the numerical approximation of the non integer derivative
- E_c: concrete Young's modulus
- K_1, K_2: elastic constants of the rheological model (see Fig. 5)
- ν: Poisson's ratio
- $\mathcal{G}_F$: fracture energy (area below the curve of Fig. 4)
- f_t: ultimate tensile strength
- $\sigma_{F.C.T.}$: maximum principal (tensile) stress acting at the fictitious crack tip
- w: crack opening displacement (also called COD)
- COD: crack opening displacement (also called w)
- w_c: critical crack opening displacement (beyond w_c no stresses are transferred in the cohesive zone)
- V_f: aggregate volume fraction
- K_{Ic}^{hom}: fracture toughness of the homogenized material
- β: concrete microstructural parameter $\left(\beta = \frac{(K_{Ic}^{hom})^2}{E_c(1-V_f)f_t}\right)$
- $\Delta\sigma$: stress relaxation due to creep
- Δw: creep displacement
- t: time
- Δt: time step

- $\mathrm{d}\sigma_t$: stress relaxation computed in each point of the FPZ (depends on local conditions only because it is assumed w=const)
- $\mathrm{d}w_t$: creep displacement computed in each point of the FPZ (depends on local conditions only because it is assumed σ=const)
- $\mathrm{d}\sigma$: real stress increment in the FPZ (depends on global and local conditions)
- $\mathrm{d}w$: real displacement increment (depends on global and local conditions)
- H: specimen height
- P_{max}: maximum (or peak) load
- P_{cost}: constant load level during the creep phase
- $\boldsymbol{K}_T$: positive definite tangential stiffness matrix
- $\boldsymbol{C}_T$: negative definite tangential stiffness matrix
- $\boldsymbol{P}$: external load vector
- $\Delta\lambda$: load multiplier
- $\boldsymbol{Q}$: unbalanced load vector
- $\Delta\boldsymbol{u}$: displacement vector

References

[1] G. I. Barenblatt. The formation of equilibrium cracks during brittle fracture: general ideas and hypotheses. *Journal of Applied Mathematics and Mechanics*, pages 622–636, 1959.

[2] D. S. Dugdale. Yielding of steel sheets containing slits. *Journal of Mechanics and Physics of Solids*, 8:100–114, 1960.

[3] A. Hillerborg, M. Modeer, and P. E. Petersson. Analysis of crack formation and crack growth in concrete by means of fracture mechanics and finite elements. *Cement and Concrete Research*, 6:773–782, 1976.

[4] S. Santhikumar and B. L. Karihaloo. Time-dependent tension softening. *Mechanics of Cohesive-Frictional Materials*, 1:295–304, 1996.

[5] S. Santhikumar, B. L. Karihaloo, and G. Reid. A model for ageing visco-elastic tension softening material. *Mechanics of Cohesive-Frictional Materials*, 3:27–39, 1998.

[6] J. Huang and V. Li. A meso-mechanical model of the tensile behaviour of concrete. *Composites*, 20:370–378, 1989.

[7] F. P. Zhou. *Time-dependent Crack Growth and Fracture in Concrete*. PhD thesis, Report TVBM-1011, Lund University of Technology (Sweden), 1992.

[8] Z. P. Bažant and R. Gettu. Rate effects and load relaxation in static fracture of concrete. *American Concrete Institute Journal*, 89(5):456–468, 1992.

[9] A. Carpinteri, S. Valente, F. P. Zhou, G. Ferrara, and G. Melchiorri. Crack propagation in concrete specimens subjected to sustained loads. In F. H. Wittmann, editor, *Fracture Mechanics of Concrete Structures*, pages 1315–1328, Germany, 1995. Aedificatio.

[10] K. B. Oldham and J. Spanier. *The Fractional Calculus*. Academic Press, New York, 1974.

[11] A. Carpinteri and F. Mainardi. *Fractals and Fractional Calculus in Continuum Mechanics*. Springer, Wien, 1997.

[12] B. L. Karihaloo. *Fracture Mechanics and Structural Concrete*. Longman Scientific and Technical, England, 1995.

[13] M. Enelund, L. Mähler, K. Runesson, and B. Lennart Josefson. Formulation and integration of the standard linear viscoelastic solid with fractional order rate laws. *International Journal of Solids and Structures*, 36:2417–2442, 1999.

[14] P. Bocca, A. Carpinteri, and S. Valente. Mixed-mode fracture of concrete. *International Journal of Solids and Structures*, 27:1139–1153, 1991.

[15] F. Barpi, F. Chillè, L. Imperato, and S. Valente. Creep induced cohesive crack propagation in mixed mode. In D. Durban and J. R. A. Pearson, editors, *Non-Linear Singularities in Deformation and Flow*, pages 155–168, The Netherlands, 1999. Kluwer Academic Publishers.

[16] A. Carpinteri, S. Valente, F. P. Zhou, G. Ferrara, and G. Melchiorri. Tensile and flexural creep rupture tests on partially-damaged concrete specimens. *Materials and Structures*, 30:269–276, 1997.

[17] F. Barpi, G. Ferrara, L. Imperato, and S. Valente. Lifetime of concrete dam models under constant loads. *Materials and Structures*, 32:103–111, 1999.

List of Tables

Table 1: Material properties.

E (GPa)	ν (-)	$\mathcal{G}_F$ (N/m)	f_t (MPa)
36	0.10	82	2.8

Table 2: Numerical parameters.

w_c (mm)	τ_1 (s)	$\Delta t/\tau_1$ (-)	β (-)	Element size (mm)
$2.2\ 10^{-4}$	150	1/50	0.05	0.0625

List of Figures

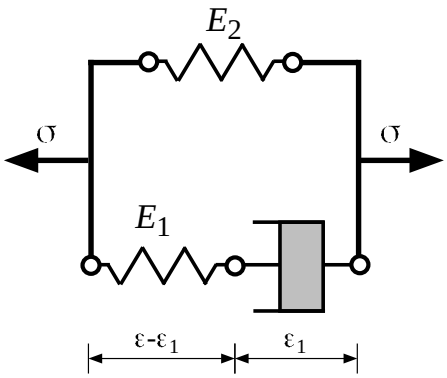

Figure 1: Rheological model.

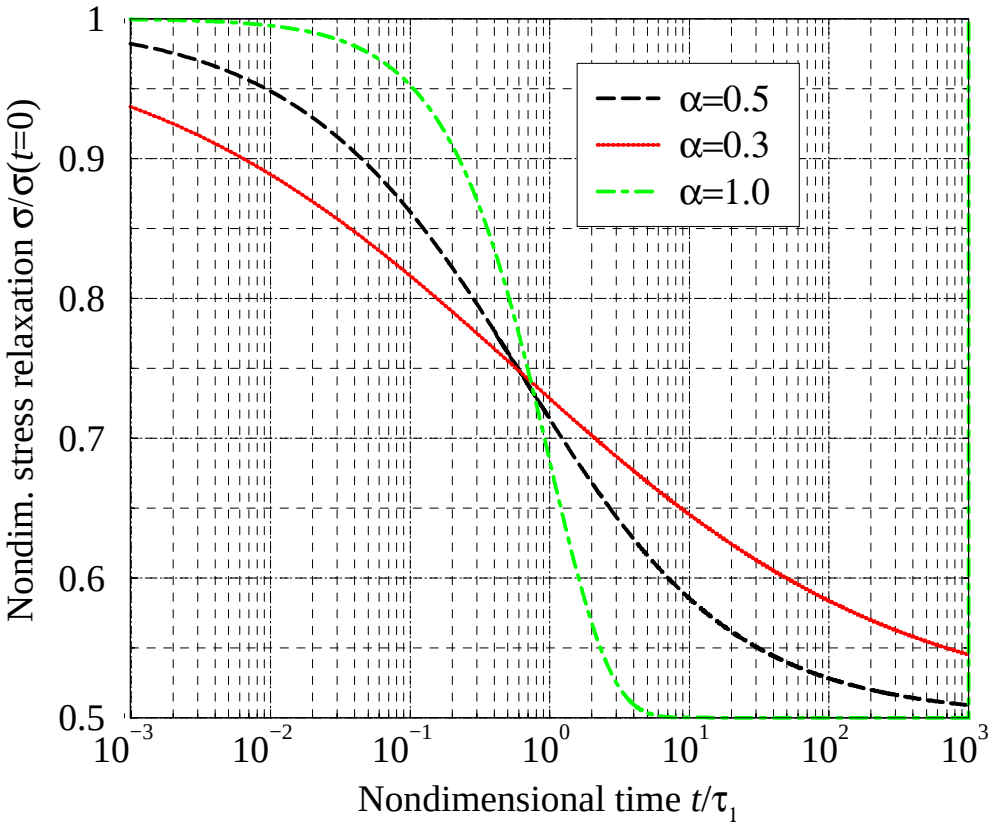

Figure 2: Stress relaxation functions ($E_1 = E_2$).

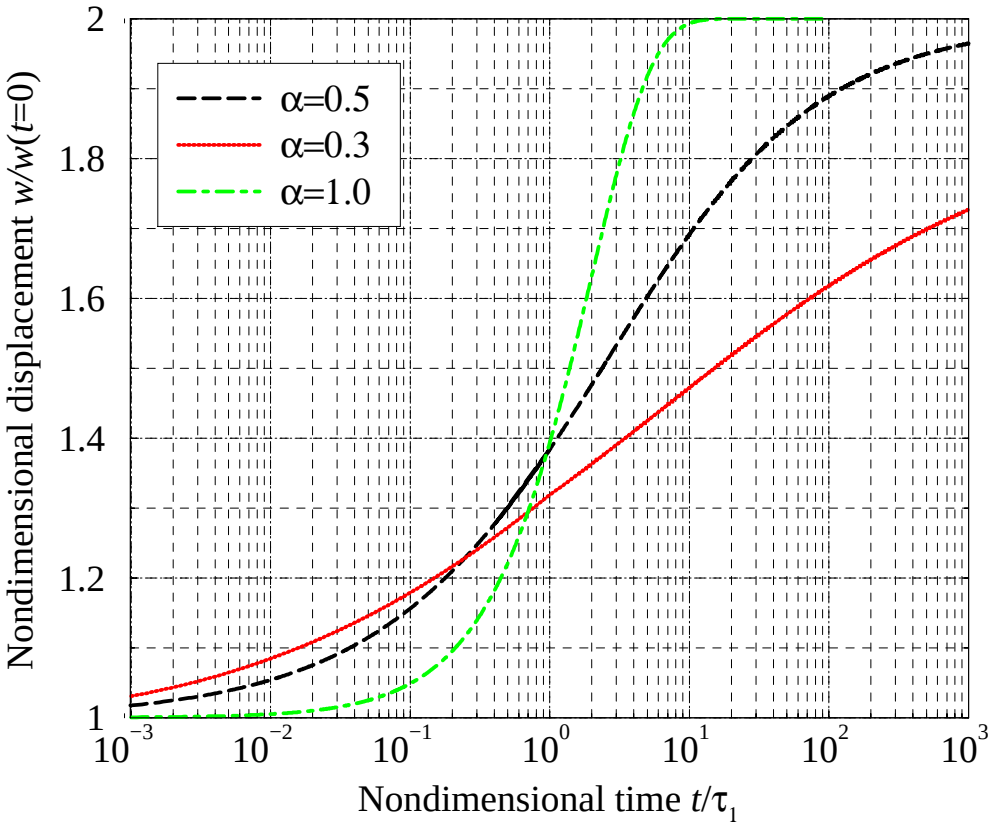

Figure 3: Creep displacement functions ($E_1 = E_2$).

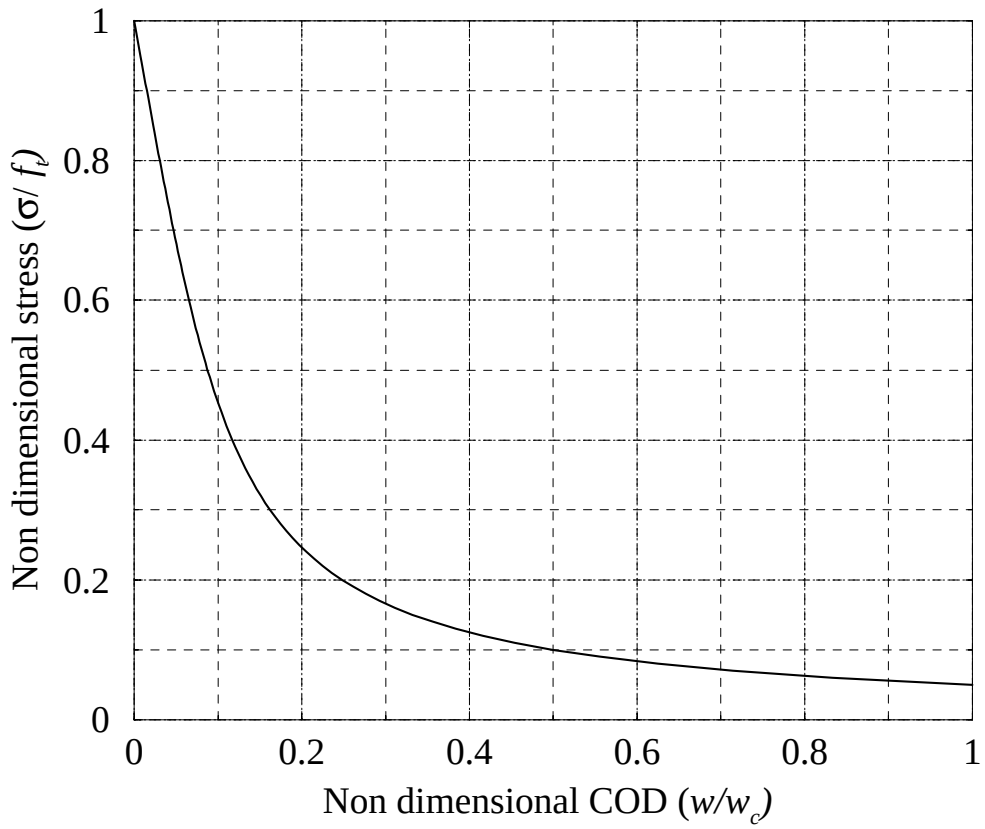

Figure 4: Cohesive stress-COD law ($\beta = 0.05$).

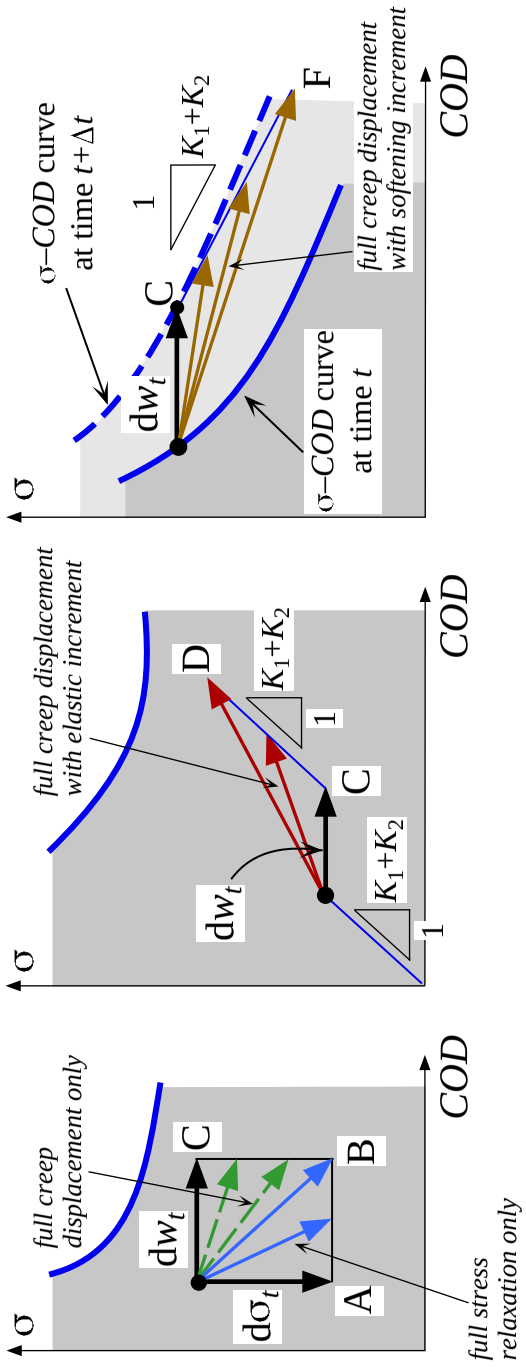

Figure 5: Stress and displacement increments during the creep phase.

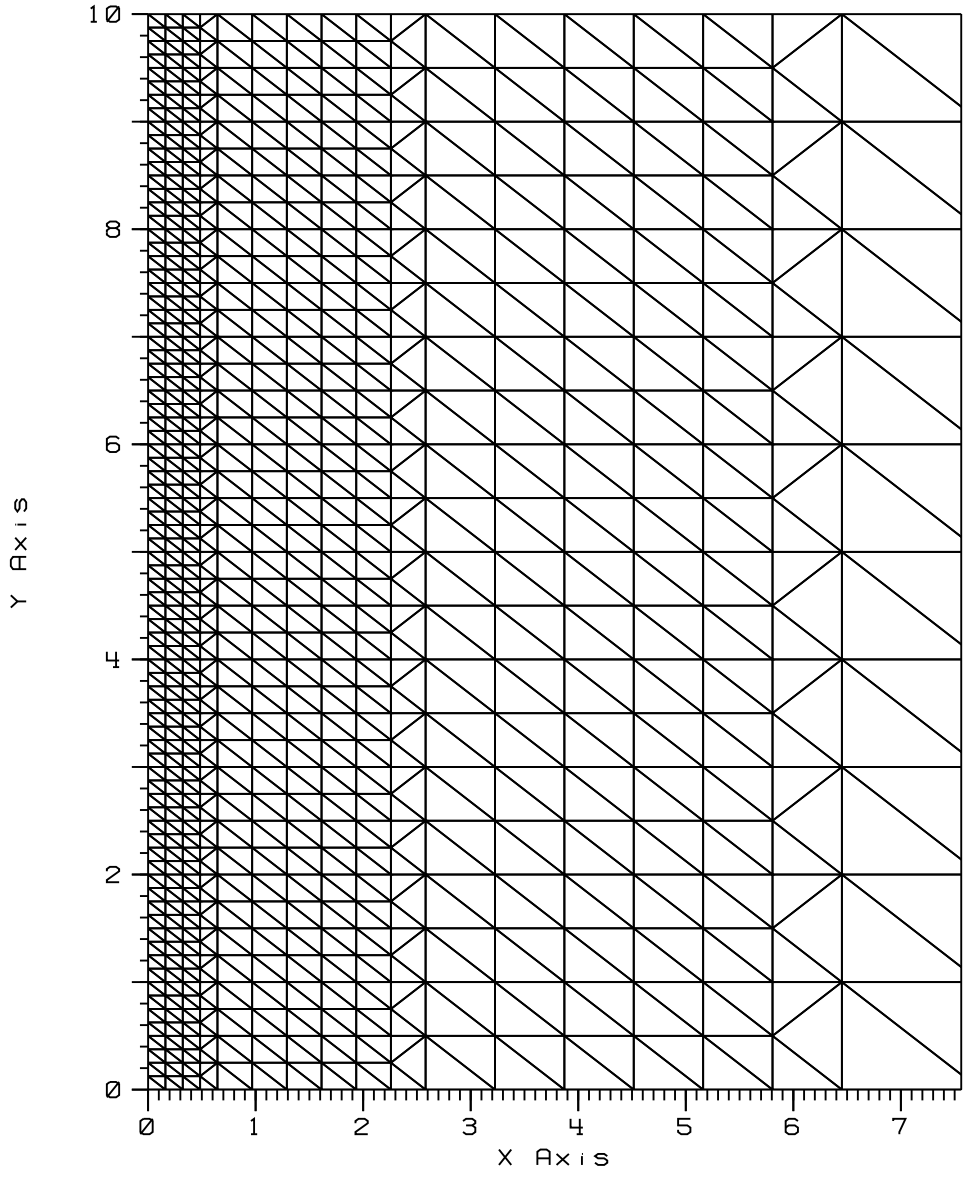

Figure 6: Portion of the finite element mesh around the symmetry axis (dimensions in centimeters).

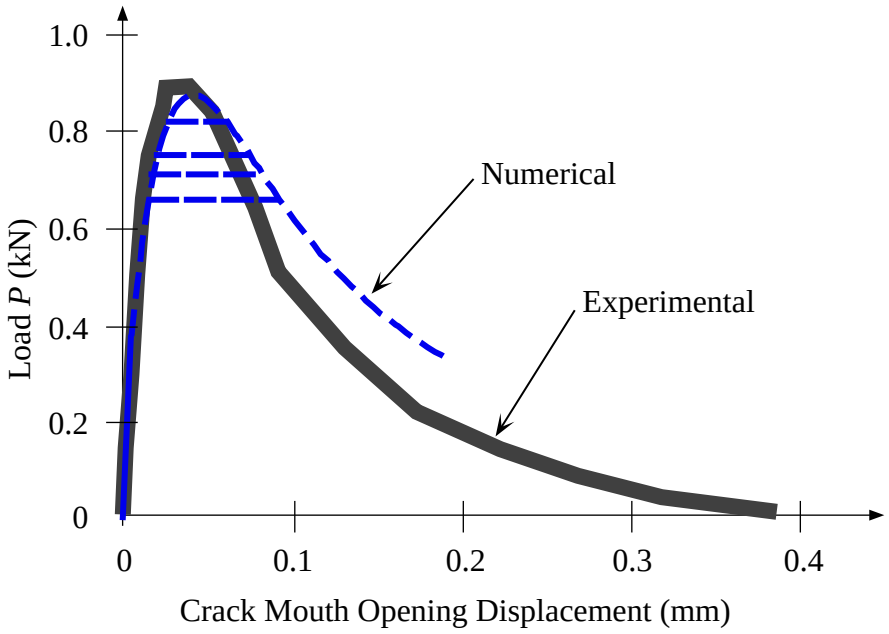

Figure 7: Experimental and numerical load vs. crack mouth opening displacement.

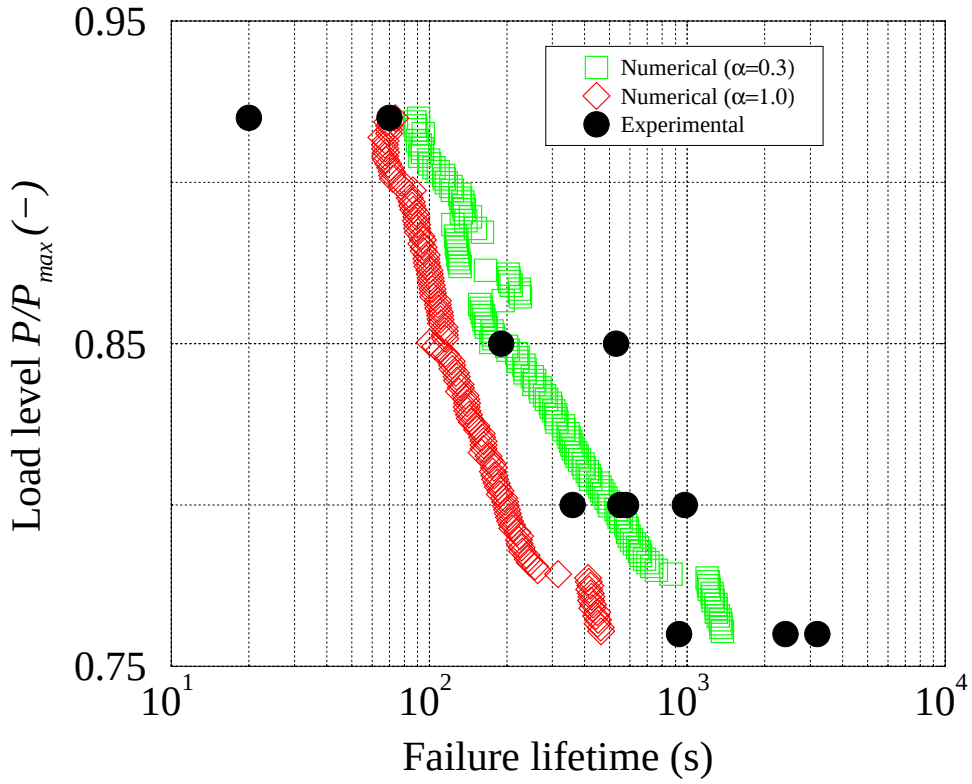

Figure 8: Comparison between experimental and numerical results in terms of failure lifetime.

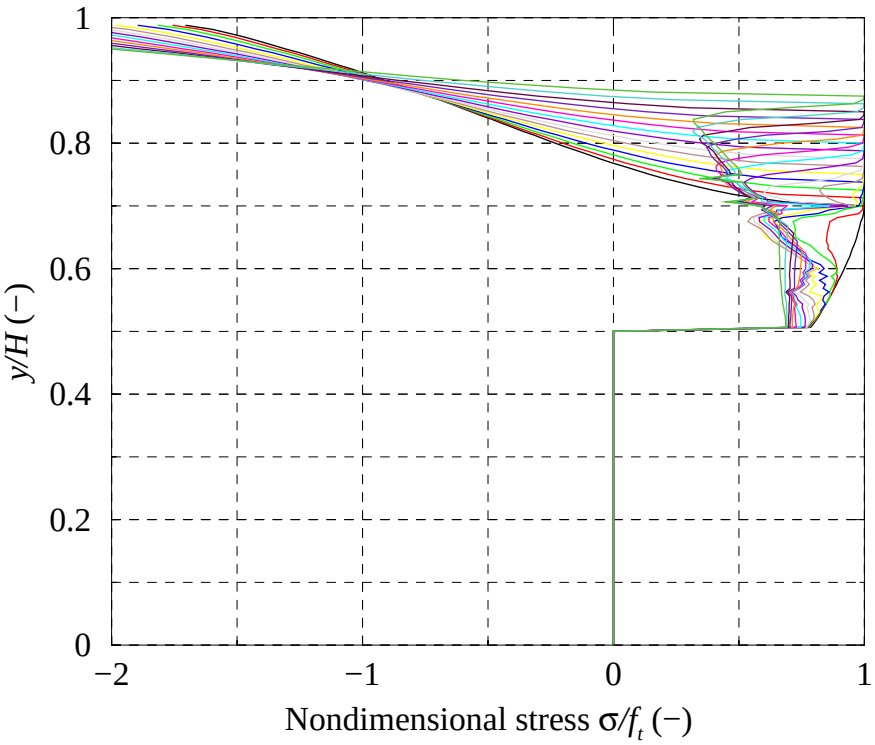

Figure 9: Stress distribution inside the process zone.

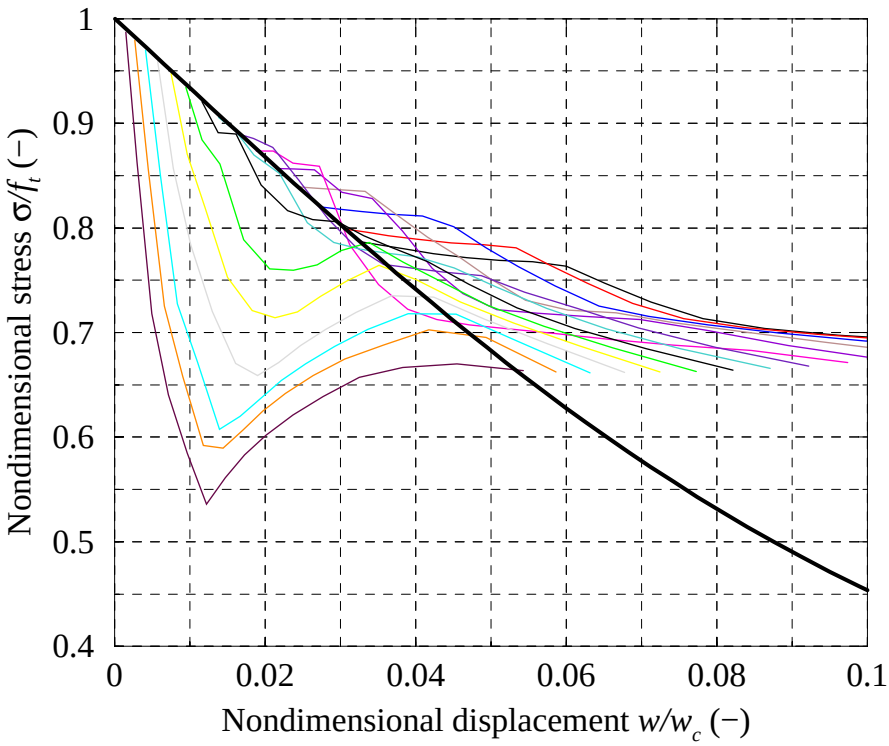

Figure 10: Stress vs. crack opening displacement paths for some points in the process zone (the thick line represnts the static envelope).

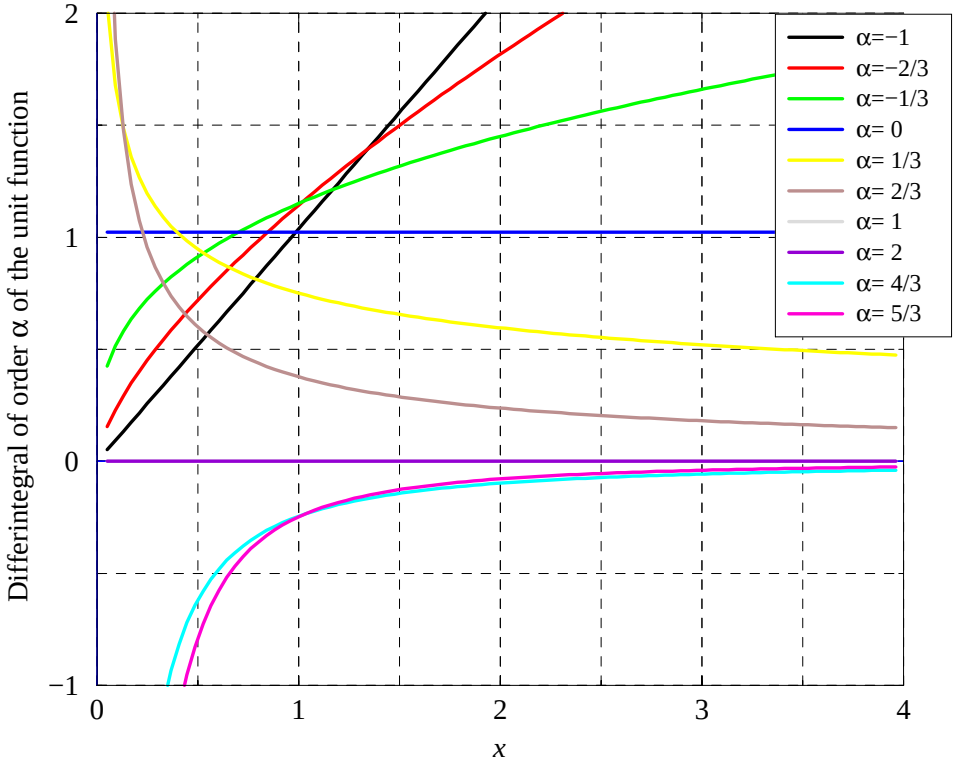

Figure 11: Derivative of order α of the unit function $y(x) = 1$.